Final Technical Report

Federal Agency and Organization: DOE EERE – Geothermal Technologies Program

Recipient Organization: Pennsylvania State University
DUNS Number: 00-340-3953
Recipient Address: 536 Deike Bld., University Park, PA 16802

Award Number: DE- EE0006762
Project Title: Leveraging a Fundamental Understanding of Fracture Flow, Dynamic Permeability Enhancement, and Induced Seismicity to Improve Geothermal Energy Production
Project Period: Oct 1, 2014 – March 31, 2018

Principal Investigator: Chris Marone
Professor
marone@psu.edu
+1.814.865.7964

Report Submitted by: PI, May 23, 2018
Project Partners: Derek Elsworth (Penn State)
Paul A. Johnson, Los Alamos National Lab

DOE Project Team:
Project Officer: William Vandermeer, 720 356 1806, william.vandermeer@ee.doe.gov
Contracting Officer: Laura Merrick, 720-356-1698, laura.merrick@ee.doe.gov
Financial Assistance Specialist: Jane Sanders, 720-356-1771, jane.sanders@ee.doe.gov
Grants Management Specialist: Edward Campbell, 720-356-1293, Edward.Campbell@ee.doe.gov
Technology Office Point of Contact: Jesse Adams

Signature C.J. Marone **Date:** 23 Jan. 2019

***The Prime Recipient certifies that the information provided in this report is accurate and complete as of the date shown.**

Acknowledgment: This material is based upon work supported by the Department of Energy's Office of Energy Efficiency and Renewable Energy (EERE) under the Geothermal Technologies Office under Award Number(s) DE-EE0006762.

Leveraging a Fundamental Understanding of Fracture Flow, Dynamic Permeability Enhancement, and Induced Seismicity to Improve Geothermal Energy Production

TABLE OF CONTENTS

---

1. EXECUTIVE SUMMARY

This project focused on assessment and discovery of fluid-rock interaction in geothermal reservoirs. We accomplished work in four main areas: 1) fracture formation and the relationship between fluid flow and shear failure, 2) assessment of fracture geometry and fluid permeability using novel acoustic measurements, 3) an improved understanding of how drilling, injection and geothermal production influence local seismicity, and 4) development of process based models for using induced seismicity to assess the critical stress-state in Earth's crust. The majority of the work involved laboratory experiments and analysis of laboratory and numerical results. We created shear fractures under true triaxial stresses designed to mimic the stress state of a geothermal reservoir and we measured fracture permeability as a function of stress state and fluid pressure under these conditions. Our work shows that fracture permeability can be altered by transient changes in stress and fluid flow. We find that fluid pressure has an unexpectedly larger impact on permeability than does applied stress and we interpret that result in terms of fracture contact area and the law of effective stress. We employ elastic waves to image fractures in the lab and develop the theory to apply our work to geothermal reservoir scale. Our work documents changes in elastic wave speed prior to earthquake-like failure in the lab and we show how the frequency magnitude distribution of microseismic lab earthquakes can be used to assess the critical stress state around faults prior to failure.

2. PROJECT GOALS, OBJECTIVES AND ACCOMPLISHMENTS

Geothermal systems require formation and exploitation of connected flow paths via hydraulic stimulation of critically stressed fractures. The ability to establish and extend a geometrically complex but highly conductive fracture network between injection and recovery wells is an essential component in the successful and repeatable development of EGS. The fracture network should be initiated and maintained with minimal induced seismicity, and the evolution of fracture permeability during the lifetime of the reservoir should be monitored and managed. Ideally, the management of fluid injection, permeability evolution, and induced seismicity would include flow enhancement and remote fracture/flow monitoring.

The evolution of permeability must satisfy two important criteria: 1) the enhancement must be significant (order microDarcy transformed to milliDarcy) to provide sufficient mass flow rates approaching the desired 100kg/s per well, and 2) the flow channels must evolve with high heat transfer area and retain efficient thermal sweep across the reservoir to prevent short-circuiting of flow and the development of cold flow paths, each of which may represent natural fracture responses to flow feedbacks during production. Effective strategies for the management of reservoir productivity require that these critical attributes of the fracture network can be developed routinely – this in turn requires that critical factors controlling fracture formation and permeability evolution are adequately understood.

Relevance and Impact of Research on Dynamic Stressing and Reservoir Permeability

In the context of fluid injection for energy production in EGS, induced seismicity is a particular concern. Earthquakes can occur in association with dynamic stresses associated with injection, reservoir temperature change, and transport of supercritical H_2O–CO_2 fluids. Such stresses are known to induce seismic activity. For certain applications, these stresses may be beneficial, via enhanced permeability, but in other ways they pose significant risk associated with accelerated deformation, fault reactivation and possible damage to the EGS reservoir.

In this project we showed that permeability enhancement can be accomplished via transient stressing. Fluid injection and dynamic stresses combine to produce significant changes in permeability, fault stability and poromechanical properties of rock. These effects are important for geothermal energy production, water management and related activities. Thus, for several reasons that are central to energy, it is important to carry on with this work and further understand how fluid injection and associated changes in stresses influence hydromechanical properties of rock and induce seismicity.

Table 1 provides a summary of tasks, accomplishments, and milestones for our project. The project had a 3-year time frame and included a 4-month no cost extension. In each of the 12 project quarters, accomplishments were in accord with plans. We published a total of 44 papers and an equal number of meeting abstracts. Details of the project plans and accomplishments are parsed into the four main research areas as described below.

Table 1

Schedule of Tasks and Milestones *Milestones M1 at end of Quarter Q1, etc	Year 1				Year 2				Year 3			
	Q1	Q2	Q3	Q4	Q5	Q6	Q7	Q8	Q9	Q10	Q11	Q12
Task 0 Cost and resource allocation for GDR/NGDS	x											
Task 1 -Permeability Evolution and Fracture Flow Management via Dynamic Stressing												
1.1 *Examine dynamic stressing on permeability evolution*												
1.1.1 Role of fluid pressures and effective stresses	M1											
1.1.2 Amplitude and frequency dependence of permeability evolution			M3	G/NG								
1.1.3 Scaling rates of permeability recovery					M5							
1.2 *Develop permeability-seismicity relations*												
1.2.1 Represent freqeuncy dependent modes of particle transport								M8				
1.2.2 Ionic and geochemical effects												
1.2.3 Chemical healing effects and permeability resetting											M11	
1.3 *Upscaled models for permeability seismicity coupling*												
1.3.1 Micro-modeling of laboratory experiments						M6						
1.3.2 DEM models for permeability evolution and upscaling												
1.4 *Linkage with field observations*									M9			
Task 2 -Acoustic Fracture Characterization and Frictional Stability												
2.1 *Development of acoustic microscope for fracture instability studies*		M2										
2.2 *Dynamic triggering under static stress conditions*				M4								
Task 3 - Dynamic Triggering												
3.1 *Dynamic triggering under direect shearing conditions*												
3.2 *Develop frictional constitutive models for triggered slip*							M7	G/NG				
3.3 *Develop process-based models for observed response*										M10		
3.4 *Develop predictive models for observed behavior and test with experimentation*												
Reports				Y1				Y2				Y3

Summary of Technical Accomplishments

We completed a broad suite of laboratory experiments and analyzed a large volume of data for each of the experiments. Our project involved developing laboratory techniques and capabilities, and training project personnel. Our project produced over 40 scientific and technical papers and included over 50 talks and presentations at scientific meetings. The accomplishments fall into four main categories. The primary manuscripts are listed here. The full list of manuscripts describing the work for this project is provided below.

1. The affect of fracture formation on fluid flow and permeability [Candela et al., 2014, 2015; Madara et al., 2016; Rivière et al., 2017; Li et al., 2017].
2. Development of an improved understanding of the relationship between fracture permeability, fluid flow, and induced seismicity in geothermal reservoirs [Scuderi et al., 2015; Fang et al., 2015; Kaproth et al., 2016; Scuderi et al., 2016; Shreedharan et al., 2017].
3. Lab earthquake prediction and assessment of precursors to failure in the form of changes in elastic properties prior to lab earthquakes [Kaproth and Marone, 2014; Scuderi et al., 2015, 2016; Tinti et al., 2017; Lubbers et al., 2018; Rouet-Leduc et al., 2018; Hulbert et al., 2019].
4. Development of numerical and process based models for induced seismicity and assessment of the critical stress-state in Earth's crust [Ikari et al., 2016; Johnson et al.,

2016; Rivière et al., 2016; Dorostkar et al., 2017; Lieou et al., 2017; Scuderi et al., 2017; Im et al., 2017, 2019].

Table 2

Experiment	Sample Type	Pore Fluid	Effective Normal Stress (MPa)	Pp_a (MPa)	Pp_b (MPa)	Oscillation Amplitude (MPa)	Oscillation Frequency
p4444	Berea	DI Water	20	3	2.8	n/a	1 Hz
p4445	Berea	DI Water	20	3	2.8	n/a	1 Hz
p4450	Berea	DI Water	20	3	2.8	0.03, 0.05, 0.07, 0.1	1 Hz
p4451	Berea	DI Water	20	3.1	2.7	0.05, 0.1, 0.2, 0.3	1 Hz
p4463	Berea	DI Water	20	3.1	2.7	0.05, 0.1, 0.2, 0.3	1 Hz
p4478	Berea	DI Water	20	3.1	2.7	0.05, 0.1, 0.2, 0.3	1 Hz
p4479	Berea	DI Water	20	3.1	2.7	200kPa	1 Hz
p4505	Westerly	DI Water	20	3.1	2.7	200kPa	1 Hz
p4506	Westerly	DI Water	20	3.1	2.7	200kPa	1 Hz
p4516	Westerly	DI Water	20	3.1	2.7	n/a	1 Hz
p4541	Westerly	DI Water	20	3.3	2.7	n/a	1 Hz
p4542	Westerly	DI Water	20	3	3	n/a	1 Hz
p4543	Westerly	DI Water	20	4	2	0.2, 0.4, 0.7, 1	1 Hz
p4571	Westerly	DI Water	20	4	2	n/a	1 Hz
p4572	Westerly	DI Water	20	4	2	0.2, 0.4, 0.7, 1	1 Hz
p4641	Berea	DI Water	20	3.3	2.7	0.05, 0.1, 0.2, 0.3	1 Hz
p4669	Berea	DI Water	20	3.2	2.8	n/a	1 Hz
p4670	Berea	DI Water	20	3.2	2.8	n/a	1 Hz
p4671	Berea	DI Water	20	3.2	2.8	0.05, 0.1, 0.2, 0.3	1 Hz
p4674	Berea	DI Water	20	3.2	2.8	0.05, 0.1, 0.2, 0.3	1 Hz
p4721	Westerly	DI Water	20	4	2	0.2, 0.4, 0.7, 1	1 Hz
p4722	Westerly	DI Water	20	4	2	0.2, 0.4, 0.7, 1	1 Hz
p4723	Westerly	DI Water	20	4	2	0.2, 0.4, 0.7, 1	1 Hz
p4724	Westerly	DI Water	20	4	2	0.2, 0.4, 0.7, 1	1 Hz
p4797	Westerly	DI Water	20	4	2	0.2, 0.4, 0.7, 1	0.3,1,10Hz
p4798	Westerly	DI Water	20	4	2	0.2, 0.4, 0.7, 1	0.1,1,10Hz

p4799	Westerly	DI Water	20	4	2	0.2, 0.4, 0.7, 1	0.1,1,10Hz
p4825	Westerly	DI Water	20	4	2	0.2, 0.4, 0.7, 1	0.1,1,10Hz
p4966	Westerly	DI Water	20.02	4	2	0.2,0.4,0.7,1	0.1,1,10Hz
p4975	Westerly	DI Water	20.02	4	2	0.01, 0.05, 0.1, 0.2, 0.4, 0.7, 1	0.1,1,10Hz
p4976	GRS	DI Water	20.02	3.1	2.9	0.01, 0.02, 0.04, 0.07, 0.1	0.1,1,10, 40Hz
p5036	Westerly	DI Water	20	3.1	2.9	0.01, 0.02, 0.04, 0.07, 0.1	0.1,1,10, 40 Hz
p5037	GRS	DI Water	20	3.1	2.9	0.01, 0.02, 0.04, 0.07, 0.1	0.1,1,10, 40 Hz
p5038	Berea	DI Water	20	3.1	2.9	N/A	0.1,1,10Hz

Task 1: Permeability Evolution & Fracture Flow Management via Dynamic Stressing

1.1 **Planned Activities**:

Summarize recent laboratory work on fracture permeability and its evolution during shear. Train project personnel in laboratory techniques. Conduct laboratory work to measure fracture permeability evolution during dynamic stressing. Carry out data analysis and develop techniques for acoustic measurements to image fracture geometry and flow. Expand the laboratory database with in-situ fracture experiments and dynamic stressing tests. Carry out detailed data analysis of permeability changes under a range of conditions. Test the acoustic data acquisition system and our technical innovations for using it to image fractures. Conduct lab tests with simultaneous measurement of fracture permeability evolution during complex stress states that include dynamic stressing. Evaluate the relationship between flow, effective stress and fracture permeability in our unusually well controlled laboratory tests. Conduct experiments to illuminate the ultrasonic properties of fractures and their evolution with shear and fluid flow. Expand the our lab database on fracture flow and dynamic permeability enhancement.

1.2 **Actual Accomplishments**: Progress was in accord with plans. We conducted 62 experiments for the project and over 20 calibration runs and tests of technical innovations. A primary focus was on permeability evolution as a function of shear slip and stress state. Experiments were performed in the configuration shown in Figure 1.

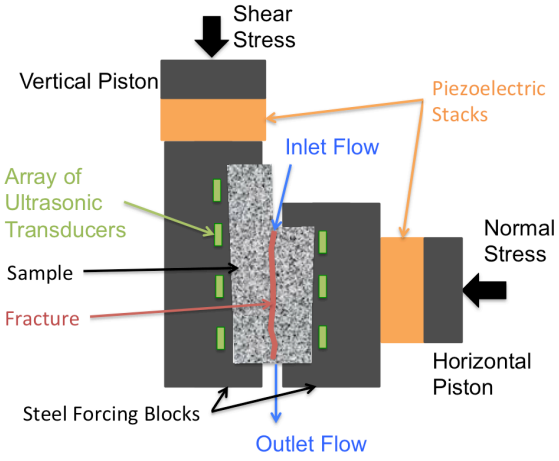

Figure 1. Test configuration for acoustic imaging during fluid flow using PZT stacks and an array of ultrasonic transducers.

Results included detailed analysis of the relationship between fracture permeability, shear slip and flow. In particular, we evaluated the role of particle clogging and shear sealing on artificial fractures. The project experiments included Berea Sandstone but focused on work using Westerly granite.

Data included measurements of permeability as a function of shear (Figure 2). These results are for fractures of Westerly Granite formed in-situ under true triaxial loading (See Fig. 1) and then subject to shear. Fractures formed dynamically with a sudden drop of shear stress. Permeability typically increased upon fracturing.

In these experiments we are studying the relationship between fracture permeability, shear and dynamic stressing. After the samples are fractured, we impose dynamic stressing via fluid pressure oscillations (Fig. 3). We looked at how dynamic stressing affected permeability and we did this as a function of shear displacement, studying permeability and the effects of dynamic stressing after shear increments of 0.1, 1.0 and 10 mm (Figure 2). We see that permeability increases after each shear increment (Figure 4) and that it then decreases with time and progressive flow during dynamic stressing.

We imposed fluid pressure oscillations to alter the effective normal stress, and we evaluated a range of stressing amplitudes from 50 to 300 kPa (Figure 3). In each case, the fluid pressure at the upper end of the fracture (Ppa) was oscillated with a given amplitude

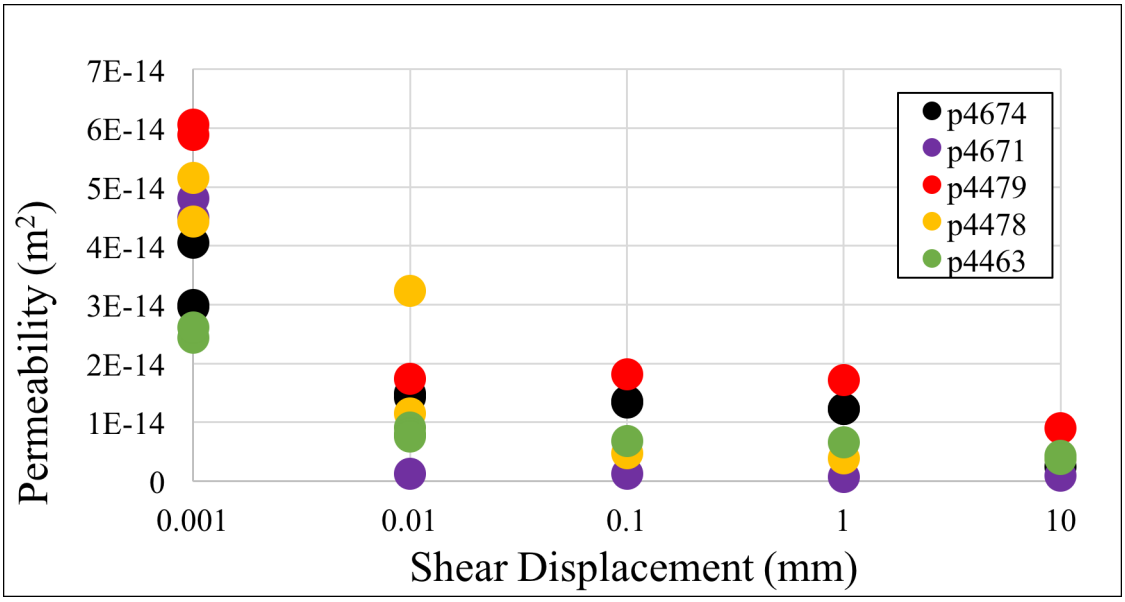

Figure 2. Fracture permeability as a function of shear load point displacement for a suite of experiments with Westerly Granite. Fractures were developed in-situ under true-triaxial loading in the configuration shown in Fig. 1 (see also the photo in Fig 8.) Fractures are rough and contain breccia when they form. Note that permeability decreases systematically with shear, indicating a set of processes that include wear, gouge formation and shear enhanced coction of the fault zone.

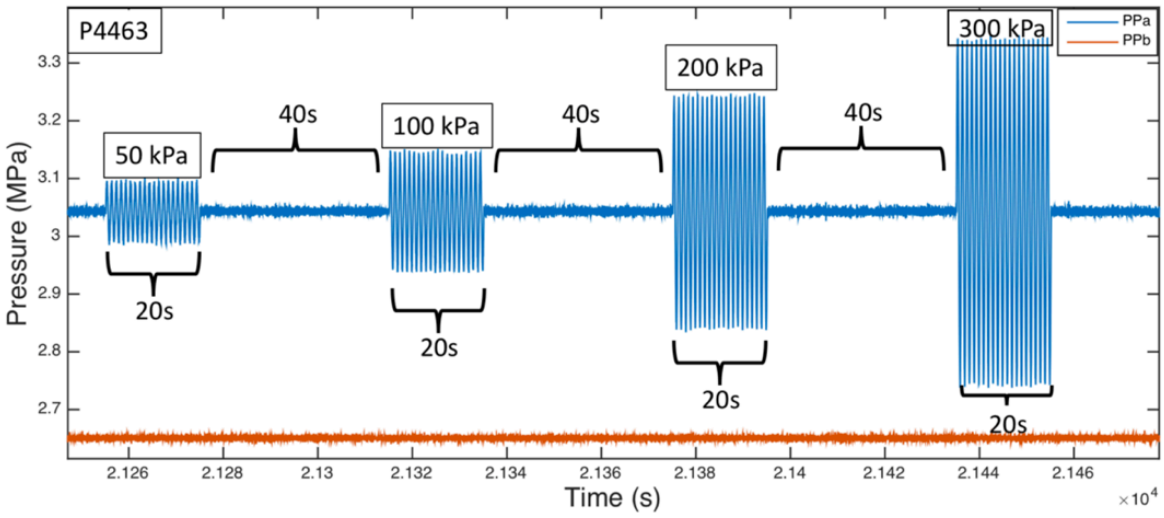

Figure 3. Fluid pressure history during dynamic stressing. Pressure is imposed along a line source at the top and bottom of the fracture. The frequency of these oscillations is 1 Hz and the duration is 20 sec. We also studied lower frequencies and longer durations. Pressure is held constant between each oscillation set. We measure permeability during these intervals.

This report is written for public disclosure and does not contain proprietary or classified information

and frequency while the downstream pressure (Ppb) was held constant via a fast acting servo controller. We measured fracture permeability before and after each set of oscillations (Figure 4). In Figure 4 we show permeability as a function of time for five sets of conditions within one experiment, which is shown in Figure 2. For example, the blue curve shows data for dynamic stressing immediately after the fracture was formed. The loading history of Figure 3 was imposed and Figure 4 shows permeability before and after each set of fluid pressure oscillations. Consistent with previous work, we found that dynamic stressing increases permeability (*Elkhoury et al.,* 2011; *Candela et al.*, 2014, 2015). In Figure 4, this is seen by coring the permeability before and after each gap, which corresponds to the time of dynamic stressing.

The permeability increases are transient but they persist over time scales, and for flow volumes, that indicate a semi-permanent character (Figure 4). Permeability decreased with time and flow immediately after fracture and after each increment of shear.

Our previous work shows that similar permeability changes for Berea Sandstone are driven by a clogging/unclogging mechanism and we are evaluating the hypothesis that a similar mechanism operates for granite.

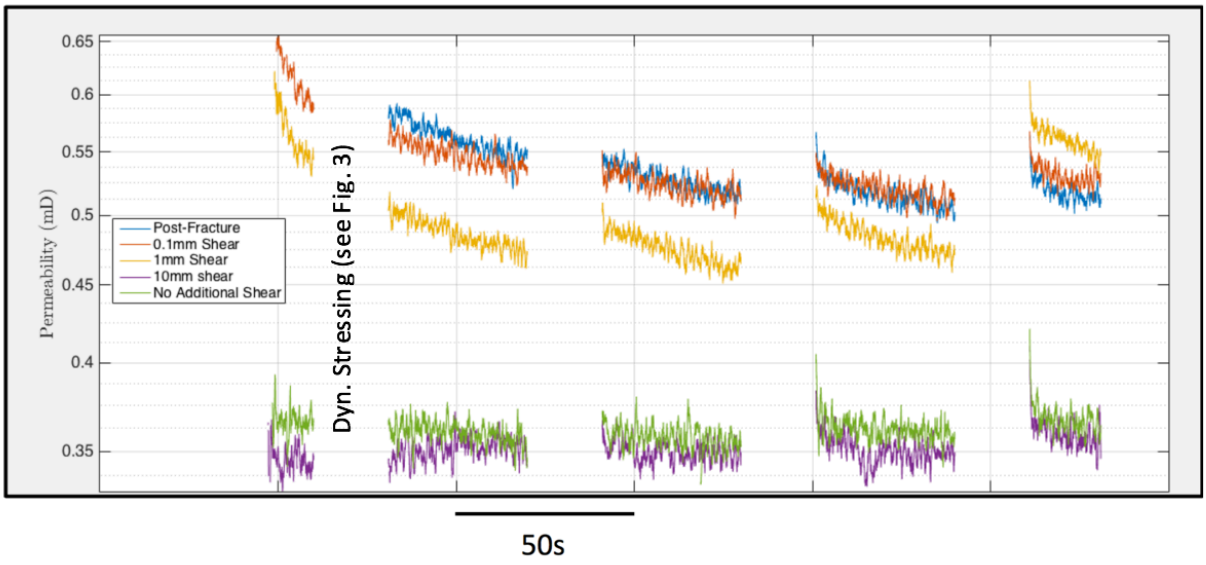

Figure 4. Permeability as a function of time for the data shown in Fig. 2. Data are shown for the times before and after the dynamic stressing history shown in Fig. 3. Gaps represent the time during which dynamic stressing occurred (the first of which is labeled). Data are shown for five phases of dynamic stressing. Note that in each case, permeability decreases with time and flow but that dynamic stressing causes a transient increase in permeability. Note that in some cases it is important to account for the trend of permeability with time when evaluating the affect of dynamic stressing. p4572

Task 2: Acoustic Fracture Characterization and Frictional Stability

2.1. **Planned Activities**: Summarize and reanalyze recent work on acoustic properties of fault zones as reported in the literature and our previous experiments. Train project personnel in laboratory techniques related to fluid flow, acoustic measurement, and data analysis. Complete training for safety, laboratory techniques, and data collection. Develop hardware and software for the acoustic imaging measurements.

2.2. **Actual Accomplishments**: Progress was in accord with plans. We conducted 62 experiments for the project and over 20 calibration runs and tests of technical innovations. We showed how to simultaneously measure permeability, friction and ultrasonic properties of fractured samples under true triaxial stresses. Figure 5 shows details of the configuration developed. This configuration allows measurement of the acoustic properties of the fracture as a function of shear and flow. One area for future work is the internal seal between the jacket and sample; this presented some difficultly due to the geometry of the samples and the pressure and electrical requirements.

These data show that the amplitude of elastic waves transmitted through nascent fractures begins to decrease well before fracture and shear. The magnitude of these changes vary systematically with ray path (Figure 6), indicating a sensitivity of elastic properties to fracture microstructure and geometry. These results show how field measurements in an EGS reservoir

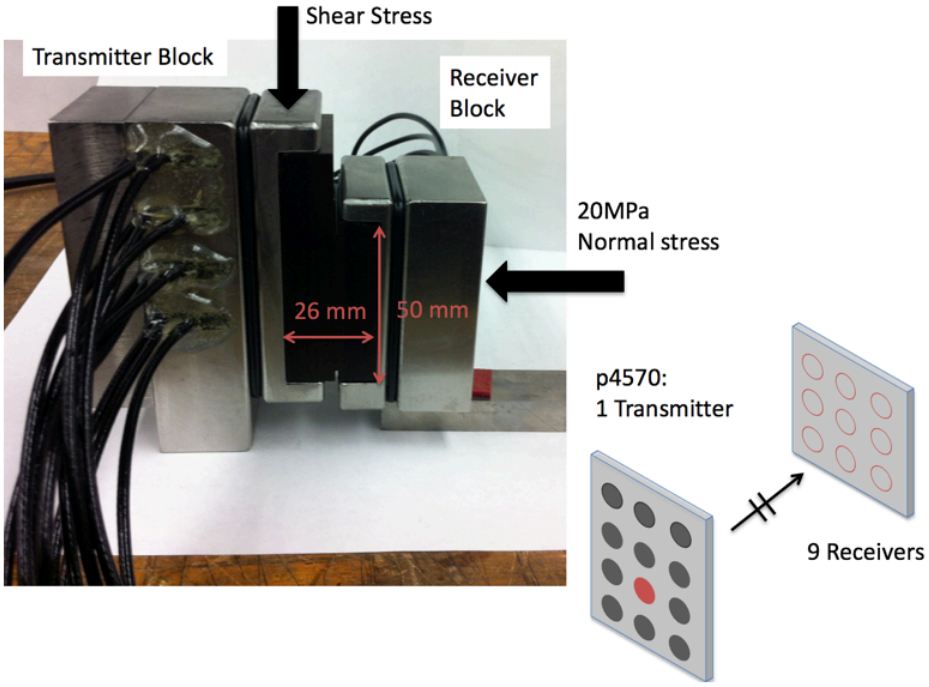

Figure 5. Loading assembly for acoustic monitoring during fracture, flow and friction measurements. The configuration includes 12 sensors on one side and 9 on the other side. We pulse each sensor on the Transmitting side and measure the signal on each of the 9 receivers. We find clear changes in elastic wave speed in association with dynamic stressing and shear.

could be used to monitor fracture properties and their evolution with flow, sealing and energy production. The lab work also shows transient changes in nonlinear elastic properties of the fractures that can be implemented in EGS production sites.

We measured the properties of natural fractures formed under true triaxial load and subject to shear. To augment these data, we also ran tests in the double direct shear configuration on bare surfaces of Westerly granite. We probed these interfaces by sending pulses every millisecond alternatively from four PZT transmitters with different polarizations (Figure 7). We used two longitudinal (P) signals and one each of shear vertical (SV) and shear horizontal (SH). Corresponding receivers record the waveforms throughout the experiment.

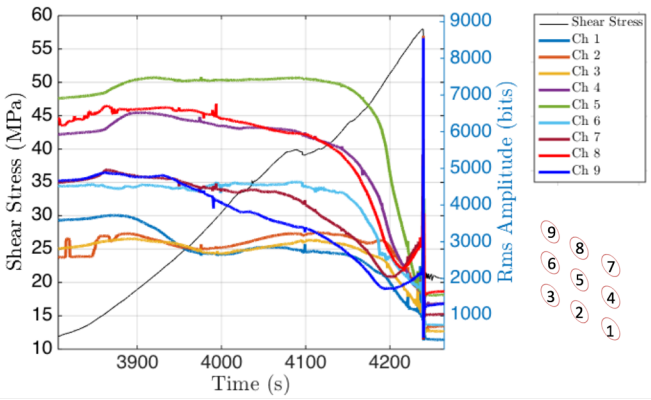

Figure 6. Shear stress and elastic wave speed as a function of time for a fracture experiment performed in the configuration shown in Fig 5. Thre fracture occurs at ~ 4230 seconds. Note that elastic wave amplitude begins to decrease well before fracture and that elastic ray paths travelling through the upper part of the fracture (channels 7, 8, 9) increase slightly just before fracture (from 4200s). Lower right inset shows receiver locations.

Figure 7 *(Rivière et al.*, 2016) shows the evolution of acoustic transmissivity as a function of fault slip during two 10×step slip velocity increases followed by a 100×step velocity decrease. The transmissivity of elastic waves (i.e., amplitude of the waveforms) decreases when the slip velocity is increased, consistent with the expectations of rate/state friction theory and asperity contact lifetime. Such changes in transmissivity are about 4-5% for a 10×step velocity, and we observe them for all polarizations. Similarly, an increase in time of flight is observed when the slip velocity is increased, which corresponds to a drop in ultrasonic velocity (not shown).

Elastic waves are therefore slower and more

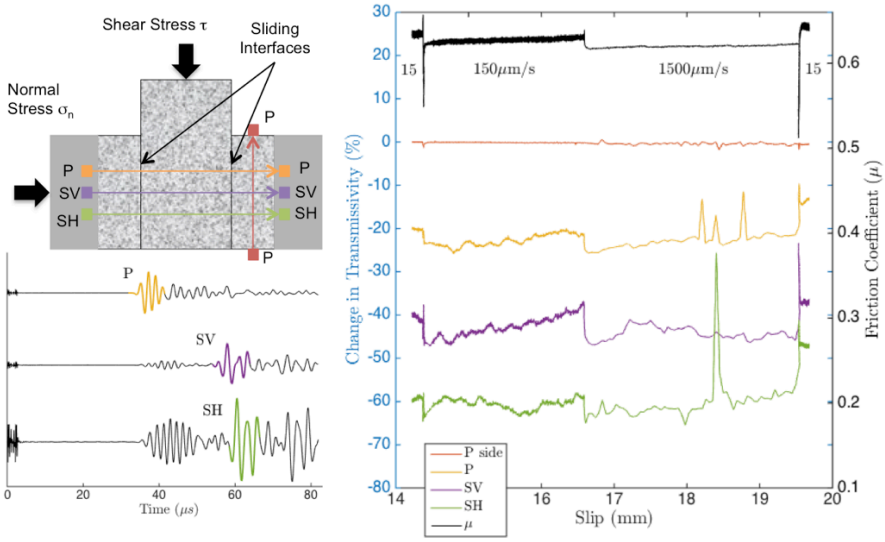

Figure 7. *Friction and acoustic data for velocity step tests on bare surfaces of Westerly granite. The experimental setup and template waveforms are shown on the left. The interfaces are probed with a P-wave and two S-waves polarized vertically (in the shearing direction) and horizontally. A fourth pair of P-wave transducers probes the side block to assess changes within the blocks. (right) Results for a step increase in load point velocity from 15 to 1500 μm/s following by a step decrease back to 15 μm/s: friction (black), change in P-wave transmissivity (red/yellow), S-wave transmissivity (purple/green) are plotted as a function of fault slip. Note the drop in transmissivity as slip velocity increases. Such changes in transmissivity will be exploited to infer the real contact area and refine our understanding of frictional processes. Such changes are about 5% for a 10×velocity step. Note that no major change occurs within the side block.*

attenuated at large slip velocities, consistent with the idea that true frictional contact area decreases with increasing sliding velocity. In addition, some long-term transient effects are also observed during the steps. Interestingly, the transmissivity of SV waves increases at 150 μm/s while all other polarizations remain rather constant. This increase suggests that interfaces are being smoothed, through breakage of asperities.

Figure 8 shows photos of the sample and loading assembly developed for in-situ fracture with simultaneous measurements of fluid permeability, friction and elastic wave properties under true triaxial stresses. The left side shows the sample after fracture, with the jacket removed. The top loading platen has 9 PZTs installed and the lower platen has 12 PZTs, each of which can be fired for active mode wave speed measurement or recorded in passive mode to monitor acoustic emission events. The right side shows the same sample as the left, with blocks separated to provide a view of the fracture plane. Fluid flow occurs along the fracture from a line source at the top and bottom of the fracture plate –that is from left to right in the photo on the left.

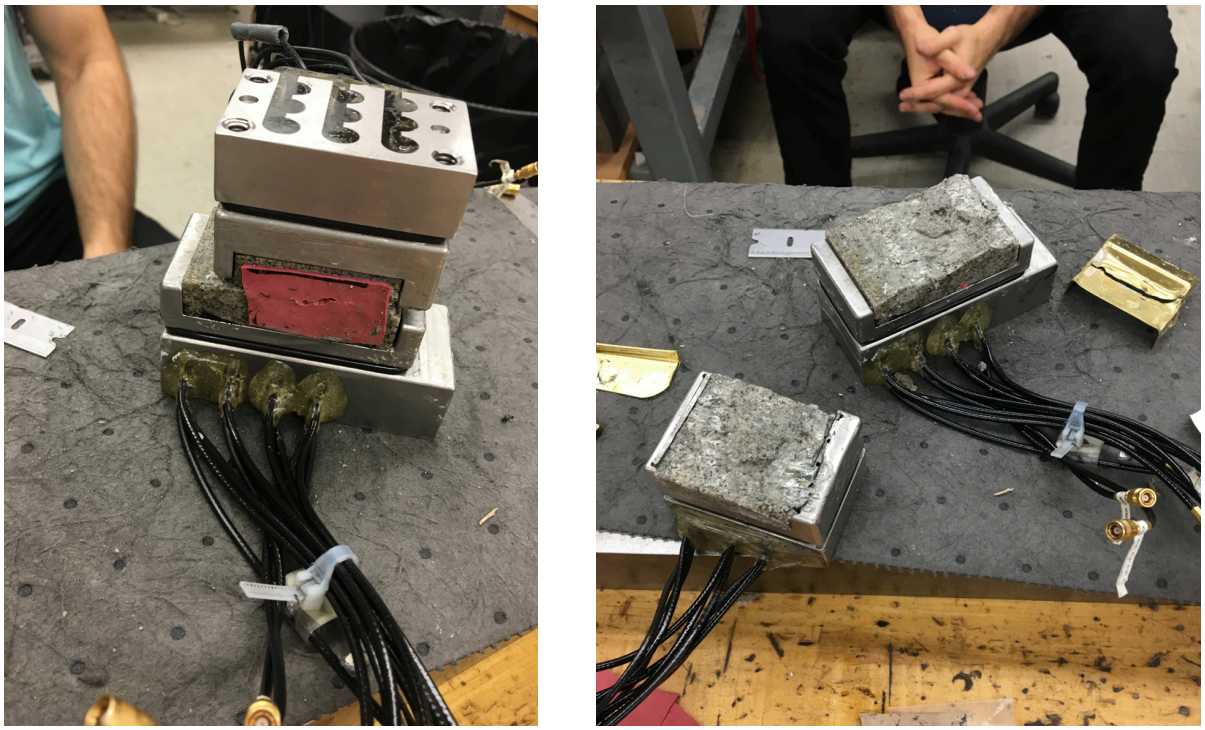

Figure 8 Photos of the sample and loading assembly for in-situ fracture with measurement of fluid permeability, friction constitutive properties and elastic wave speed.

Task 3: Dynamic Triggering and Injection Induced seismicity

3.1. **Planned Activities**: Conduct numerical models of dynamic triggering using a Discrete Element Method (DEM). Study the role of communition and fragmentation of wear materials within fractures and sheared fault zones. Document the nature of energy accumulation and release during the earthquake nucleation and rupture. Develop the capability to compare DEM results with lab experiment data on stick-slip. Shed light on the physical mechanisms that are involved in induced earthquakes with particular focus on the dynamics of sheared granular fault gouge.

3.2. **Actual Accomplishments**: Our accomplishments were in accord with plans. Results of this part of our work are published in several manuscripts. In the numerical experiments, we subjected faults to transient dynamic stresses and investigated the physics of earthquake triggering (Figure 9). We find that at a critical vibrational amplitude (strain) there is an abrupt transition from negligible time-advanced slip (clock advance) to full clock advance. This work also focused on acoustically-induced slip in wet and dry sheared granular layers. We showed how dynamic stressing and fluids can induce seismicity and trigger earthquake-like failure. Lab results on precursory behaviors prior to shear failure were detailed in several publications, including [*Marone et al.*, 2015; Riviere et al., 2016, 2018; Scuderi et al., 2015]. In the lab, we developed methods to produce repetitive, slow stick-slip, analogous to slow earthquakes [*Leeman et al.*, 2016, 2018; *Scuderi et al.*, 2016].

A key element of our activities in Task 3 was the development and use of a three-dimensional discrete element model to study stick-slip failure in a saturated granular layer designed to simulate wear material in a fracture or fault gouge in a tectonic setting (Figure 9). The fracture surface and granular fault gouge consistent of 8000 particles with a poly-disperse size distribution. At very low fluid content, fluids impose cohesive and viscous forces on particles. Our simulations show that by increasing the fluid content and pressure, friction increases and the fault failure interval during shear shows a higher recurrence time between failure events (Figure 10). Failure events also exhibit larger stress drop and greater compaction when fluid lubricated compared to dry. We

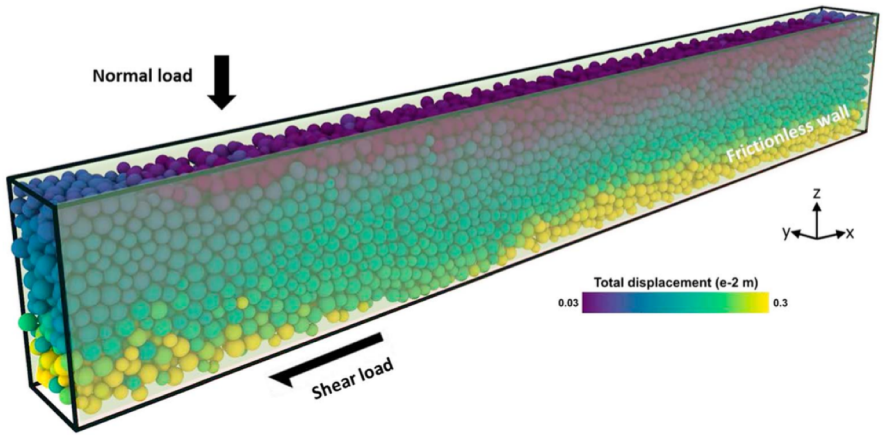

Figure 9. Model fault zone for study of shear and earthquake-like stick-slip friction. Color-coding shows total particle displacement (sum of three components). Particle diameter ranges between 90 and 150 μm. A vertical load confines the layer (*z* direction) and remains constant during shear. A displacement control mechanism is employed to shear the sample in *x* direction with constant velocity of 600 μm/s (after *Dorostkar et al.*, 2017)

demonstrate that a small volume of fluid induces cohesive forces between wet grains that are responsible for an increase in intergranular coordination number leading to greater shear stability. Stabilization is indicated by a lowering of the system kinetic energy for wet shear compared to dry. In lab experiments, the physicochemical processes are related to pressure solution and hydromechanical effects of cohesion. Our work illuminates the role of particle interactions and demonstrate the conditions under which granular processes and fluids impact fault zone processes, including slip initiation, weakening, and failure.

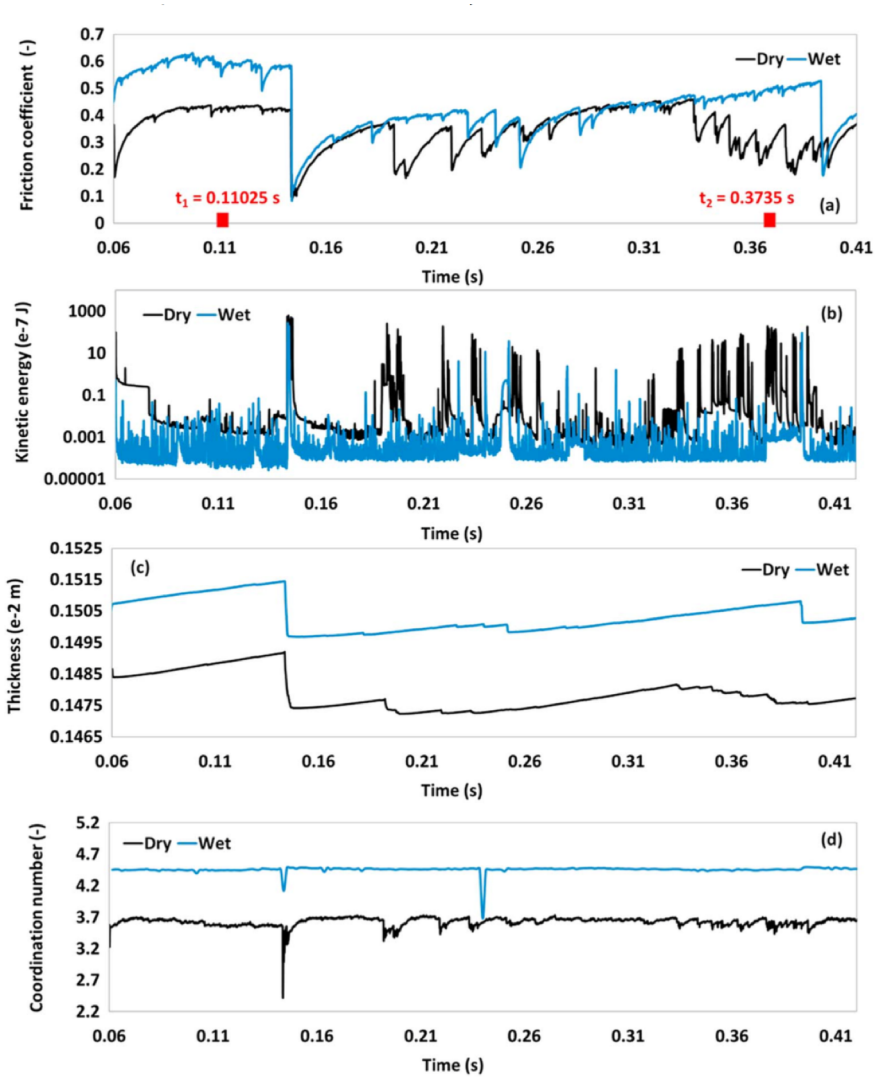

Figure 10. DEM simulation results showing (a) friction coefficient, (b) kinetic energy, (c) layer thickness and (d) average coordination number for dry and fluid saturates samples sheared under a stress of 300 kPa. (after *Dorostkar et al.*, 2017)

Task 4: Using induced seismicity to assess the critical stress-state in Earth's crust

4.1. **Planned Activities**: Conduct laboratory and numerical experiments to study induced seismicity and earthquake precursors. Investigate how microearthquakes can be used to monitor the approach to fault zone failure and probe the critically-stressed state in Earth's crust. Test these models using AE during shear loading and characterize the correlation between AE generated at different stages of shear stress as large-scale fault failure is approached.

4.2. **Actual Accomplishments**: Our accomplishments were in accord with plans. The main results focused on lab earthquake prediction and observations of precursors to earthquake-like failure. Results of this part of our work are published in several manuscripts. We showed that continuous records of fault zone acoustic emissions (AE), corresponding to microearthquakes, can predict lab earthquakes. In the experiments, elastic waves are recorded by piezoelectric (PZT) crystals embedded in the shear assembly (Figure 12). The AE signals exhibit systematic changes in frequency-magnitude statistics during the lab seismic cycle consistent with Gutenberg-Richter scaling. However, the signals also contain previously unrecognized information that is like tectonic tremor and low frequency earthquakes as observed on tectonic faults. We developed machine learning (ML) approaches and found that both fast and slow labquakes are preceded by AE signals that foretell catastrophic failure (Figure 12). Fast lab earthquakes are associated with impulsive release of acoustic wave energy, while slow failure events are preceded by low-amplitude tremor. In all cases, the acoustic energy appears to be essentially featureless during the early stages of the lab seismic cycle; however ML can discern and illuminate a predictive signal (Figure 12). We are currently working to expand these activities and apply them to ML in Geothermal systems via a new project.

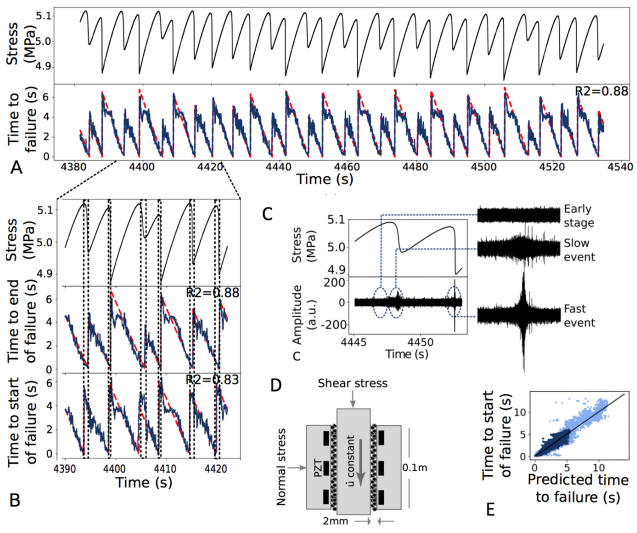

Figure 12. Laboratory earthquake prediction. (A) Shear stress for slow and fast labquakes with time to failure (red line) and ML predictions (blue). Note strong correlation between measurement and prediction. (B) Detail of predicted (blue lines) and measured failure times (red lines) for both long and short events. (C) Shear stress and acoustic amplitude during load-up and failure. Early stage elastic waves look like noise, but ML finds a predictive signal. (D) Double-direct shear configuration with PZTs used to record elastic waves. (E) Predicted vs. measured event times for a large number of slow and fast lab quakes. The black diagonal corresponds to a perfect prediction. (Modified from Hulbert et al., 2018)

PROJECT OUTPUT

Publications:

1. Bhattacharya P., Rubin, A. M., Bayart, E., Savage, H. M., and C. Marone, Critical evaluation of state evolution laws in rate and state friction: fitting large velocity steps in simulated fault gouge with time-, slip- and stress-dependent constitutive laws, *J. Geophys. Res. Solid Earth*, *120*, 10.1002/2015JB012437, 2015.
2. Candela, T., Brodsky, E. E., Marone C., and D. Elsworth, Laboratory evidence for particle mobilization as a mechanism for permeability enhancement via dynamic stressing, *Earth and Plan. Sci. Lett.,* **392**, 279-291, 10.1016/j.epsl.2014.02.025, 2014.
3. Candela, T., E. E. Brodsky, C. Marone, and D. Elsworth, Flow rate dictates permeability enhancement during fluid pressure oscillations in laboratory experiments, *J. Geophys. Res. Solid Earth*, 120, 2037–2055, doi:10.1002/ 2014JB011511, 2015.
4. Carpenter, B. M., D. M. Saffer, and C. Marone, Frictional properties of the active San Andreas Fault at SAFOD: Implications for fault strength and slip behavior, *J. Geophys. Res. Solid Earth*, 120, 5273–5289, 10.1002/ 2015JB011963, 2015.
5. Carpenter, B. M., Ikari, M. J., and C. Marone, Laboratory observations of time-dependent frictional strengthening and stress relaxation in natural and synthetic fault gouges, *J. Geophys. Res. Solid Earth*, 121, 1183–1201, 10.1002/ 2015JB012136, 2016.
6. Dorostkar, O., Guyer, R. A., Johnson, P. A., Marone, C. and J. Carmeliet, On the role of fluids in stick-slip dynamics of saturated granular fault gouge using a coupled computational fluid dynamics-discrete element approach, *J. Geophys. Res. Solid Earth,* 122, 3689–3700, 10.1002/2017JB014099, 2017.
7. Dorostkar, O., Guyer, R. A., Johnson, P. A., Marone, C. and J. Carmeliet, On the micromechanics of slip events in sheared, fluid saturated fault gouge, *Geophys. Res. Lett*., GRL56055, 10.1002/2017GL073768, 2017.
8. Dorostkar, O., Guyer, R. A., Johnson, P. A., Marone, C., and J. Carmeliet, Cohesion-induced stabilization in stick- slip dynamics of weakly wet, sheared granular fault gouge. *J. Geophys. Res. Solid Earth*, *123*, 2115–2126, 10.1002/ 2017JB015171, 2018.
9. Fang, Y., den Hartog, S. A. M., Elsworth, D., Marone, C. and T. Cladouhos, Anomalous distribution of microearthquakes in the Newberry geothermal reservoir: mechanisms and implications, *Geothermics*, 10.1016/j.geothermics.2015.04.005, 2015.
10. Ferdowsi, B., Griffa, M., Guyer, R. A., Johnson, P. A., Marone, C., and J. Carmeliet, Acoustically-induced slip in sheared granular layers: application to dynamic earthquake triggering, *Geophys. Res. Lett., 42,* 9750–9757*,* 10.1002/201Fer5GL066096, 2015.
11. Gan, Q., Elsworth, D., Alpern, J., Marone, C., and P. Connelly, Breakdown Pressures due to infiltration and exclusion in finite length boreholes, *J. of Petrol. Sci. & Eng.*, *127,* 329-337, 10.1016/j.petrol.2015.01.011, 2015.
12. Hulbert, C., Rouet-Leduc, B., Johnson, P. A., Ren, C. X., Rivière, J., Bolton, D. C., and C. Marone, Machine learning predictions illuminate similarity of fast and slow laboratory earthquakes, *Nat. Geosc.*, 12, 69-74, 10.1038/s41561-018-0272-8, 2019.
13. Ikari, M. J., B. M. Carpenter, and C. Marone, A microphysical interpretation of rate- and state-dependent friction for fault gouge, *Geochem. Geophys. Geosyst.*, 17, 1660–1677, 10.1002/2016GC006286, 2016.

14. Ikari, M., A. Niemeijer, and C. Marone, Experimental investigation of incipient shear failure in foliated rock *J. Struct. Geol., 77,* 82-91*,* 10.1016/j.jsg.2015.05.012*,* 2015.
15. Im, Kyungjae, Elsworth, D., Marone, C. and J. Leeman, The impact of frictional healing on stick-slip recurrence interval and stress drop: Implications for earthquake scaling, *J. Geophys. Res. Solid Earth,* 122, 10.1002/2017JB014476, 2017.
16. Im, Kyungjae, Marone, C. and D. Elsworth, The transition from steady frictional sliding to inertia-dominated instability with rate and state friction, *J. Mech. Phys. Sol.*, 10.1016/j.jmps.2018.08.026, 2019.
17. Ishibashi, T., Elsworth, D., Fang, Y, Rivière, J., Madara, B., Asanuma, H., Watanabe, N. and C. Marone, Friction-stability-permeability evolution of a fracture in granite, *Water Resources Res*., 10.1029/2018WR022598 2018.
18. Johnson, P. A., J. Carmeliet, H. M. Savage, M. Scuderi, B. M. Carpenter, R. A. Guyer, E. G. Daub, and C. Marone, Dynamically triggered slip leading to sustained fault gouge weakening under laboratory shear conditions, *Geophys. Res. Lett*., 43, 1559–1565, 10.1002/ 2015GL067056, 2016.
19. Kaproth, B. M., Kacewicz, M. Muhuri, S. and C. Marone, Permeability and frictional properties of halite-clay-quartz faults in marine-sediment: The role of compaction and shear, *Marine and Petroleum Geology*, *78*, 222-235, 10.1016/j.marpetgeo.2016.09.011, 2016.
20. Kumar, K., Elsworth, D., Mathews, J. P. and C. Marone, Permeability evolution analogies in sorbing media: a corison between organic-rich shale and coal, *GeoFluids*, 10.1111/gfl.12135, 1-13, 2015.
21. Leeman, J. R., M. M. Scuderi, C. Marone, and D. M. Saffer, Stiffness evolution of granular layers and the origin of repetitive, slow, stick-slip frictional sliding, *Granular Matter*, 10.1007/s10035-015-0565-1, 2015.
22. Leeman, J. R., Marone, C. and D. M. Saffer, Frictional mechanics of slow earthquakes, *J. Geophys. Res. Solid Earth*, 123, 10.1029/2018JB015768, 2018.
23. Leeman, J. R., Saffer, D. M., Scuderi, M. M., and C. Marone, Laboratory observations of slow earthquakes and the spectrum of tectonic fault slip modes. *Nature. Commun*. 7:11104, 10.1038/ncomms11104, 2016.
24. Li, X., Feng, Z., Han, G., Elsworth, D., Marone, C., and D. Saffer, Hydraulic fracturing in shale with H_2O, CO_2 and N_2, *American Rock Mechanics Association, USRMS*, 2015.
25. Li, X., Feng, Z., Han, G., Elsworth, D., Marone, C., Saffer, D., and D. S. Cheon, Breakdown pressure and fracture surface morphology of hydraulic fracturing in shale with H_2O, CO_2 and N_2, *Geomechanics and Geophysics for Geo-energy and Geo-Resources, 2, 63-76,* 10.1007/s40948-016-0022-6, 2016.
26. Li, X., Feng, Z., Han, G., Elsworth, D., Marone, C., Saffer, D., and D. S. Cheon, Permeability evolution and proppant compaction in artificial fractures on Green River shale. *American Rock Mechanics Association, 16-833, USRMS,* 2016.
27. Li, Xiang, Feng, Z., Han, G., Elsworth, D., Marone, C., Saffer, D., and D. S. Cheon, Permeability evolution of propped artificial fractures in Green River Shale, *Rock Mech. and Rock Eng.*, 50, 1473-1485, 2017.

28. Lieou, C. K. C., Daub, E. G., Guyer, R. A., Ecke, R. E., Marone, C. and P. A. Johnson, Simulating stick-slip failure in a sheared granular layer using a physics-based constitutive model, *J. Geophys. Res. Solid Earth,* JGRB51945, 10.1002/2016JB013627*,* 2017.
29. Lubbers, N., Bolton, D. C., Mohd-Yusof, J. Marone, C., Barros, K. and P. A. Johnson, Earthquake catalog-based machine learning identification of laboratory fault states and the effects of magnitude of completeness, *Geophys. Res. Lett*., 45, 13,269–13,276, 10.1029/2018GL079712, 2018.
30. Marone, C. and D. M. Saffer, The mechanics of frictional healing and slip instability during the seismic cycle, In Treatise on Geophysics (Second Edition), edited by Gerald Schubert, Elsevier, Oxford, 10.1016/B978-0-444-53802-4.00092-0, pp. 111-138, 2015.
31. Marone, C. and E. Richardson, Connections between fault roughness, dynamic weakening, and fault zone structure, *Geology*, 10.1130/focus012016.1, 2016.
32. Marone, C., Training machines in Earthly ways, *Nature Geosc.,* 11, 301-302, 2018.
33. Rivière, J., Lv, Z., Johnson, P. A., and C. Marone, Evolution of *b*-value during the seismic cycle: Insights from laboratory experiments on simulated faults, *Earth and Plan. Sci. Lett.,* 482, 407–413, 10.1016/j.epsl.2017.11.036, 2018.
34. Rivière, J., Pimienta, L., Scuderi, M., Candela, T., Shokouhi, P., Fortin, J., Schubnel, A., Marone C., and P. A. Johnson, Frequency, pressure and strain dependence of nonlinear elasticity in Berea sandstone, *Geophys. Res. Lett*., 2016.
35. Rouet-Leduc, B., Hulbert, C., Bolton, D. C., Ren, C. X., Rivière, J., Marone C., Guyer, R. A., and P. A. Johnson, Estimating fault friction from seismic signals, *Geophys. Res. Lett*., 10.1002/2017GL076708, 2018.
36. Ryan, K. L., Rivière, J. and C. Marone, The role of shear stress in fault healing and frictional aging, *J. Geophys. Res. Solid Earth,* 2018.
37. Scuderi, M. M., B. M. Carpenter, P. A. Johnson, and C. Marone, Poromechanics of Stick-Slip Frictional Sliding and Strength Recovery on Tectonic Faults, *J. Geophys. Res. Solid Earth*, 10.1002/2015JB011983, 2015.
38. Scuderi, M. M., Collettini, C. and C. Marone, Frictional stability and earthquake triggering during fluid pressure stimulation of an experimental fault, *Earth and Plan. Sci. Lett., 477,* 84–96*,* 10.1016/j.epsl.2017.08.009, 2017.
39. Scuderi, M. M., H. Kitajima, B. M. Carpenter, D. M. Saffer, and C. Marone, Evolution of permeability across the transition from brittle failure to cataclastic flow in porous siltstone, *Geochem. Geophys. Geosyst.*, 16, 10.1002/2015GC005932, 2015.
40. Scuderi, M. M., Marone, C., Tinti, E., Di Stefano, G., and C. Collettini, Precursory changes in seismic velocity for the spectrum of earthquake failure modes, *Nature Geosc.,*, doi:10.1038/ngeo2775, 2016.
41. Scuderi, M. M., Viti, C., Tinti, E., Collettini, C. and C. Marone, Evolution of shear fabric in granular fault gouge from stable sliding to stick-slip and implications for fault slip mode, *Geology*, 10.1130/G39033.1, 2017.
42. Shreedharan, S., Rivière, J., Bolton, C., Zheng, L., Johnson, P. A., and C. Marone, Characterization of Acoustic Emissions From Laboratory Stick-Slip Events in Simulated Fault Gouge. American Rock Mechanics Association, ARMA-2017-0362*, USRMS*, 2017.

43. Tinti, E., Scuderi, M. M., Scognamiglio, L. Di Stefano, G., Marone, C., and C. Collettini, On the evolution of elastic properties during laboratory stick-slip experiments spanning the transition from slow slip to dynamic rupture, *J. Geophys. Res. Solid Earth*, 10.1002/2016JB013545, 2016.
44. Wojatschke, J., Scuderi, M. M., Warr, L. N., Carpenter, B. M., Saffer, D., and C. Marone, Experimental constraints on the relationship between clay abundance, clay fabric and frictional behavior for the Central Deforming Zone of the San Andreas Fault, *Geochem. Geophys. Geosyst.*, 10.1002/2016GC006500, 2016.